IEEE Access
Multidisciplinary | Rapid Review | Open Access Journal

Received July 2, 2019, accepted July 17, 2019, date of publication July 19, 2019, date of current version October 9, 2019.

Digital Object Identifier 10.1109/ACCESS.2019.2930101

Kinematic Characteristics and Dynamics Analysis of an Overconstrained Scissors Double-Hoop Truss Deployable Antenna Mechanism Based on Screw Theory

BO HAN[1], DONG ZHENG[1], YUNDOU XU[1,2], JIANTAO YAO[1,2], AND YONGSHENG ZHAO[1,2]

[1]Parallel Robot and Mechatronic System Laboratory of Hebei Province, Yanshan University, Qinhuangdao 066004, China
[2]Key Laboratory of Advanced Forging and Stamping Technology and Science of Ministry of National Education, Yanshan University, Qinhuangdao 066004, China

Corresponding author: Yongsheng Zhao (yszhao@ysu.edu.cn)

This work was supported in part by the National Natural Science Foundation of China under Grant 51675458, in part by the Key Project of Natural Science Foundation of Hebei Province of China under Grant E2017203335, and in part by the Higher Education Youth Top Talent Project of Hebei Province of China under Grant BJ2017060.

ABSTRACT Large diameter space deployable antenna is the key equipment for communication and data transmission between spacecraft and base stations on earth. Based on the overconstrained scissors mechanism, a double-hoop truss deployable antenna mechanism is constructed in this paper, which can be used as the antenna support mechanism for satellites and other spacecraft, and its kinematic characteristics and dynamics are analyzed based on screw theory. First, the configuration and the overconstrained features of the double-hoop truss deployable mechanism are analyzed with the truss mechanism divided into a plurality of mechanism units. The geometric conditions for the double-hoop form are also investigated with the consideration of joint size effects. Then, based on the screw theory, the degree of freedom (DOF) of the mechanism is analyzed, showing that this mechanism has only one DOF. Next, the velocity and acceleration of the components in the mechanism are examined. Through the screw and screw derivatives operation, the velocities and accelerations of the components and the Jacobian matrixes are obtained. Finally, a dynamic model of the double-hoop truss deployable mechanism is established based on the Newton–Euler equation and the principle of virtual work, and this model is verified by the numerical calculation and simulation verification. The overconstrained scissors double-hoop truss deployable antenna mechanism proposed in this paper has a good application prospect in the field of space deployable antennas, and the theoretical analysis method in this paper can provide insights into other complex spatial deployable mechanisms.

INDEX TERMS Overconstrained mechanism, scissors mechanism, double-hoop truss deployable antenna, screw theory, kinematics, dynamics.

I. INTRODUCTION

As various types of spacecraft become increasingly large and complex, deployable mechanisms have received considerable attention because they can be stored in a folded state during transportation, occupy a small space of the carrier, and can also be fully deployed when required to work [1]–[6]. An important application of deployable mechanisms is deployment and support for the large-diameter satellite antennas in space [7], such as the deployable antenna on the Russian "Soyuz" spacecraft, the space antenna of the Japanese ETS-VIII satellite, the American AstroMesh deployable antenna, and the SAR antenna of the Chinese HJ-1-C satellite [8]–[11]. The deployable mechanism has thus become a popular research topics in the field of satellite antennas.

The deployable mechanism belongs to the spatial multiple closed-loop mechanism. Some researchers have carried out a series of studies on the configuration design of the deployable mechanism, and have obtained a variety of new deployable mechanisms. Lu et al. constructed a planar deployable antenna mechanism based on the Hoekens unit

The associate editor coordinating the review of this manuscript and approving it for publication was Rosario Pecora.

mechanism with linear output [12]; Vu et al. constructed a variety of deployable mechanisms based on the pyramidal deployable unit mechanism [13]. After studying the application of Bricard and Bennett linkage mechanisms in space deployable mechanisms, Chen et al. developed a variety of large-scale deployable mechanisms [14]–[16]. Qi et al. constructed a deployable antenna mechanism based on the Myard mechanism [17], and Han et al. developed a plurality of pyramid deployable mechanisms based on the spatial symmetric 7R mechanism (R representing the revolute joint) [18]. References [19]–[23] examined the application of scissors mechanism in space deployable mechanisms; Guan et al. constructed several tetrahedral truss and hoop truss deployable antenna mechanisms [24]–[28]; Deng et al. studied the type synthesis method for large deployable mechanisms, building several deployable antenna mechanisms [29]–[31]; Zhao et al. studied the planar deployable linkage and its application in overconstrained lift mechanisms [32]. The mechanisms constructed by these studies are mostly suitable for space antennas with diameters less than 10 m. When the space antenna has a large diameter, hoop or double-hoop truss deployable mechanism is mostly used at present.

Degree of freedom (DOF) is the most basic parameter for a mechanism. It is thus necessary to analyze the DOF of a deployable mechanism before its application [33]–[35]. The traditional formula for DOF analysis is the Grübler-Kutzbach (G-K) formula [36], but it has been proved unsuitable for overconstrained mechanisms [37]. This problem is being solved with the continuous development and application of screw theory. Huang et al. proposed a modified G-K formula, which has been proved suitable for almost all existing mechanisms [38], and Zhao et al. studied the DOF of planar scissors mechanism combinations [39]. A link-demolishing and equivalent method for the tetrahedral truss deployable antenna mechanism was proposed by Xu et al. based on screw theory [40]. Based on both screw theory and graph theory, Wei *et al.* [41] and Sun *et al.* [42] analyzed the mobility of Hoberman switch-pitch ball and its variant, and the mobility of scissors mechanism combinations respectively. These studies discussed in detail the analysis process of using screw theory to calculate the DOF of spatial mechanisms, which provides a good reference for the DOF analysis in this paper.

As an efficient analytical tool, screw theory can also be used to analyze the kinematics and dynamics of various mechanisms. Gallardo et al. have studied the application of screw theory in the kinematics analysis of parallel mechanisms [43]–[46], and combined them with the principle of virtual work to solve dynamics problems in the subsequent studies [47]–[49]. References [50] and [51] studied the velocity and acceleration of lower mobility parallel mechanisms based on screw theory. Based on screw theory, Zhao *et al.* [52] and Sun *et al.* [53] studied the kinematics and dynamics of Hessian matrix of parallel mechanisms, and of the scissor deployable mechanism unit, respectively. These studies analyzed the kinematics and dynamics of parallel mechanisms with several branches or deployable mechanism unit with only a small number of joints and rods, there are few research on complex spatial truss deployable mechanisms.

The studies mentioned above provide a useful reference for relevant research of deployable mechanisms. In recent years, many studies about deployable mechanisms have focused on the configuration design and structural analysis, and due to their complexity, the studies on the kinematics and dynamics analysis are mostly by simulation, there are few theoretical derivations. Screw and screw derivatives can clearly and simply indicate the velocity and acceleration of a rigid body, thus suitable for kinematics and dynamics analysis of complex spatial mechanisms, and we can use them to analysis the deployable truss mechanisms.

This study proposes a double-hoop truss deployable antenna mechanism based on the overconstrained scissors mechanism, and analyzes the kinematic characteristics and dynamics of the mechanism proposed, drawing on screw theory. The rest of this paper is organized as follows. In Section II, the configuration design and overconstrained features analysis are described, and the geometric conditions for the double-hoop form are analyzed. Section III presents the DOF analysis of the double-hoop truss deployable mechanism, Section IV and Section V present the analysis of velocity and acceleration, respectively. In Section VI, a dynamic model of the double-hoop truss deployable mechanism is introduced, and verified by numerical simulation. Conclusions are given in Section VII.

II. CONFIGURATION DESIGN AND GEOMETRIC CONDITION ANALYSIS OF THE OVERCONSTRAINED SCISSORS DOUBLE-HOOP TRUSS DEPLOYABLE ANTENNA MECHANISM

A. CONFIGURATION DESIGN AND ANALYSIS

The overconstrained scissors double-hoop truss deployable mechanism proposed in this study is shown in Fig. 1. It is composed of two hoop truss deployable mechanisms and a plurality of connected scissors mechanism units. The two hoop truss deployable mechanisms consist of a plurality of overconstrained scissors mechanisms, with the configurations of the inner hoop and the outer hoop being the same, but with different sizes of the two hoops.

Fig. 1 shows the fully folded state and the fully deployed state of the double-hoop truss deployable mechanism. The overconstrained scissors mechanism unit is a central symmetric mechanism used to assemble the inner hoop and the outer hoop, and the connected scissors mechanism unit is an asymmetric mechanism. The half deployed state of the two scissors mechanism units are shown in Fig. 2.

The overconstrained scissors mechanism unit is composed of a symmetric scissors mechanism and two 3R mechanisms. They are connected by the nodes, the four axes on the end of the scissors mechanism are collinear with the four axes on the two 3R mechanisms, as shown in Fig. 3.

The scissors mechanism shown in Fig. 3 is a planar mechanism, which can move only in a plane due to the

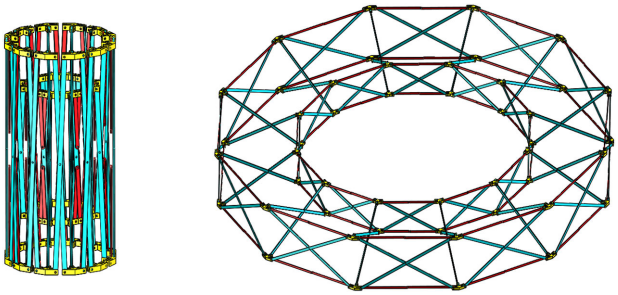

FIGURE 1. Overconstrained scissors double-hoop truss deployable mechanism.

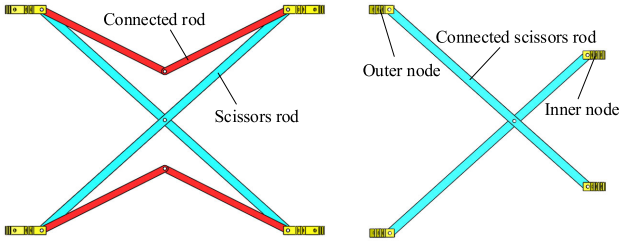

FIGURE 2. Overconstrained scissors mechanism unit and the connected scissors mechanism unit.

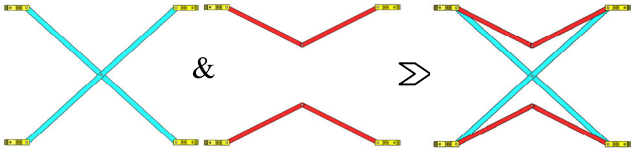

FIGURE 3. Overconstrained scissors mechanism unit and its components.

constraints provided by the joints. The relative motion trajectory between the adjacent endpoints is a straight line. The 3R mechanism is also a planar mechanism without constraints on the movement in the plane and considered as a redundant branch. When combined with the scissors mechanism and two 3R mechanisms to construct the overconstrained scissors mechanism unit, the four endpoints in the overconstrained scissors mechanism unit show the same motion characteristics as those of the single scissors mechanism. The scissors mechanism and the 3R mechanism provide repeated constraints on the four nodes located at the ends of the mechanism unit, so that the combined mechanism unit shown in Fig. 3 is an overconstrained mechanism unit. The double-hoop truss deployable mechanism composed of the mechanism units is also an overconstrained mechanism.

The existence of the overconstraints have no effect on the movement of the double-hoop truss deployable mechanism, but they can greatly improve the stiffness of the whole mechanism. When the two connected rods in a 3R mechanism move to the collinear position, the whole mechanism reaches the fully deployed state, and this state is also a border singular position for the whole mechanism, as shown in Fig. 4. If a force is applied to the mechanism in the vertical direction, the transmission angle of the mechanism at this position

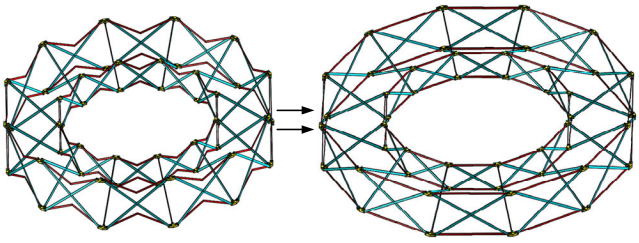

FIGURE 4. Half deployed state and fully deployed state of the double-hoop truss deployable mechanism.

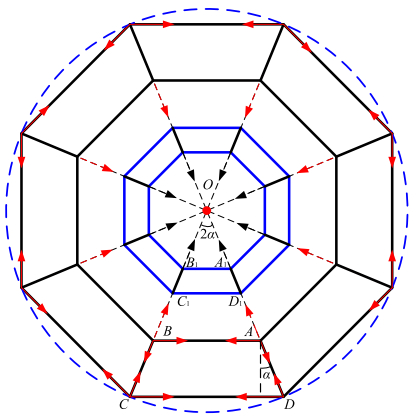

FIGURE 5. Folding process of the double-hoop truss deployable mechanism.

is 0°, the pressure angle is 90°, none of the joints can move, and the whole mechanism degenerates to a stable structure. The structure can rely on the individual rods to counteract the external force, and does not need to provide additional driving torque on the joint. Thus, the whole mechanism has high structural stiffness and load capacity.

B. ANALYSIS OF GEOMETRIC CONDITIONS

The planar projection schematic diagram of the double-hoop truss deployable mechanism and its folding process are shown in Fig. 5, it can be seen as a planar polygon combined by a plurality of isosceles trapezoids, the more number of mechanism units, the closer it is to a hoop. During the folding process of the whole mechanism, the vertices of the plane polygon moving close to each other, accompanied by the process of the vertices moving to the center, and finally the adjacent vertices coincide and moves together to the center point.

As shown in Fig. 5, the two nodes on each side of the unit $ABCD$ move close to each other during the folding of the mechanism, with the unit folded into unit $A_1B_1C_1D_1$, and then folded to the minimum state. The other units have the same folding process. The center angle corresponding to the unit $ABCD$ shown in Fig. 5 is 2α. In order to ensure the double-hoop form of the truss mechanism, the symmetry of the scissors mechanism and the size of the nodes are considered. The lengths and angle of the scissors rods are shown in Fig. 6.

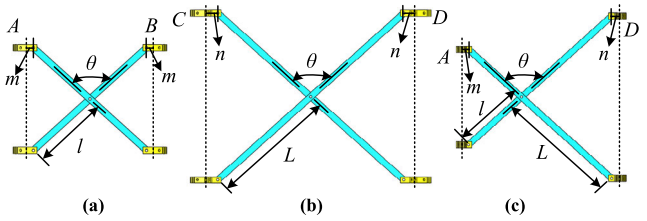

FIGURE 6. Geometric features of the scissor mechanism unit. (a) Inner scissors mechanism. (b) Outer scissors mechanism. (c) Connected scissors mechanism.

As shown in Fig. 6, the angle in each scissors mechanism is θ, the rod lengths of inner and outer scissors mechanisms are $2l$ and $2L$, respectively, R joint is located in the middle position of each rod, and the length of the rod in the connected scissors mechanism is $l + L$ with the rod divided in two parts by the R joint, and with the lengths being l and L, respectively. Given the size of the nodes, the distance between the rotation axis and the center on the inner node is m, and the distance between the rotation axis and the center on the outer node is n.

The following equations can be obtained from Fig. 5:

$$\begin{cases} CD = AB + 2AD\sin\alpha \\ AD = (AB + CD)/2 \end{cases} \tag{1}$$

Fig.6 can yield the following relationships:

$$\begin{cases} AB = 2l\sin(\theta/2) + 2m \\ CD = 2L\sin(\theta/2) + 2n \end{cases} \tag{2}$$

Based on Eq. (1) and Eq. (2), the following equation can be obtained:

$$\frac{AB}{CD} = \frac{1-\sin\alpha}{1+\sin\alpha} = \frac{l\sin(\theta/2)+m}{L\sin(\theta/2)+n} \tag{3}$$

Eq. (3) can be written as:

$$l\sin(\theta/2) + m = L\sin(\theta/2)\frac{1-\sin\alpha}{1+\sin\alpha} + n\frac{1-\sin\alpha}{1+\sin\alpha} \tag{4}$$

Eq. (4) is a complex equation. Instead of finding a general solution, we are interested in a particular solution which makes the terms on the left side equal the corresponding terms on the right side. Hence, instead of Eq. (4), the following equations are solved:

$$\begin{cases} l\sin(\theta/2) = L\sin(\theta/2)\dfrac{1-\sin\alpha}{1+\sin\alpha} \\ m = n\dfrac{1-\sin\alpha}{1+\sin\alpha} \end{cases} \tag{5}$$

Based on Eq. (5), the proportional relationship can be obtained:

$$\frac{l}{L} = \frac{m}{n} = \frac{1-\sin\alpha}{1+\sin\alpha} \tag{6}$$

Angle α in Fig. 5 is related to the number of the sides in the whole double-hoop truss deployable mechanism. If the number of sides is N, the following equation can be obtained:

$$2\alpha = 360/N \tag{7}$$

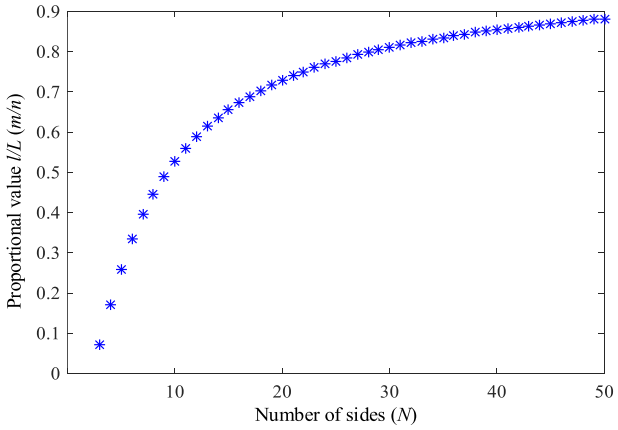

FIGURE 7. Proportional relationship between rod lengths and the number of scissors mechanism units.

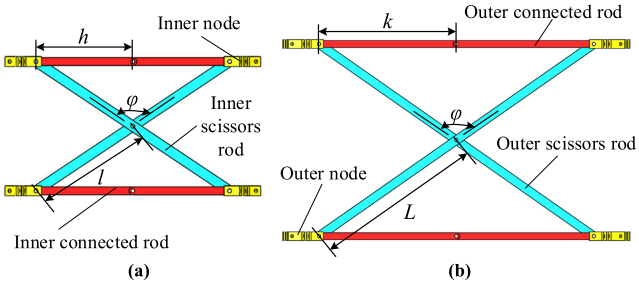

FIGURE 8. Fully deployed overconstrained scissors mechanism units. (a) Inner overconstrained scissors mechanism. (b) Outer overconstrained scissors mechanism.

Substituting Eq. (7) into Eq. (6), we can get the final relationship between the inner scissors rods and outer scissors rods for the double-hoop form of the whole deployable mechanism:

$$\frac{l}{L} = \frac{m}{n} = \frac{1-\sin(180/N)}{1+\sin(180/N)} \tag{8}$$

Eq. (8) shows the proportional relationship of the inner scissors rods and outer scissors rods are related to the number of sides in the whole mechanism. With the Matlab software, the expressions in Eq. (8) can be plotted as Fig. 7.

It can be seen from Fig. 7 that with the increase of the number of sides in the double-hoop truss deployable mechanism, the proportion value increases, though always less than 1. That is, although the length difference becomes smaller, the length of the inner scissors rod is always shorter than that of the outer scissors rod. When the overconstrained scissors mechanism is fully deployed, the connected rods in the 3R mechanism between the adjacent nodes reach a collinear position, and the angle between the two scissors rods reaches the maximum value, as shown in Fig. 8.

The angle in each overconstrained scissors mechanism shown in Fig. 8 is φ, and the lengths of the connected rods between the adjacent nodes are h and k. The following

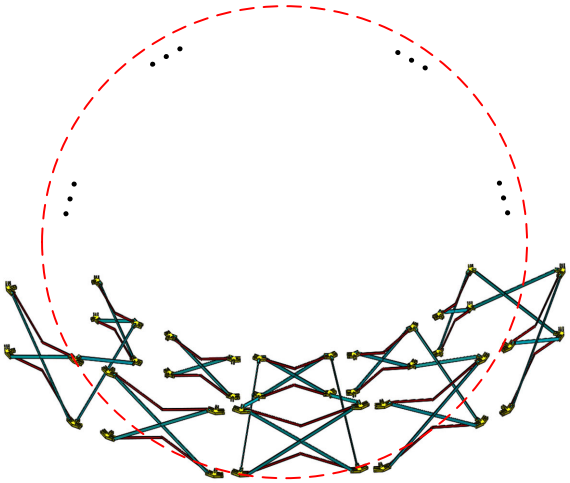

FIGURE 9. Structural decomposition of the double-hoop truss deployable mechanism.

equations can then be obtained from Fig. 8:

$$\begin{cases} h = l\sin(\varphi/2) \\ k = L\sin(\varphi/2) \end{cases} \tag{9}$$

Since l and L satisfy Eq. (8), the relationship of the lengths h and k can be obtained:

$$\frac{h}{k} = \frac{1-\sin(180/N)}{1+\sin(180/N)} \tag{10}$$

From Eq. (8) and Eq. (10), we can see that the scissors rods and the connected rods in the inner and outer overconstrained scissors mechanisms have the same proportional relationship, both of which are related to the number of sides in the double-hoop truss deployable mechanism.

III. DOF ANALYSIS OF THE DOUBLE-HOOP TRUSS DEPLOYABLE MECHANISM

When the number of sides in the double-hoop truss deployable mechanism is N, the mechanism in the half deployed state can be divided into a plurality of mechanism units, as shown in Fig. 9.

It can be seen from Fig. 9 that the double-hoop truss deployable mechanism can be divided into one closed-loop deployable mechanism unit, two overconstrained scissors mechanism units, and a plurality of non-closed-loop deployable mechanism units with the number of N-2. An analysis of the DOF of the mechanism units can reveal the DOF of the whole mechanism.

A. DOF ANALYSIS OF THE CLOSED-LOOP DEPLOYABLE MECHANISM UNIT

As shown in Fig. 10, a coordinate system O-XYZ is established for the closed-loop deployable mechanism unit, and each node is numbered with an uppercase letter. The origin of the coordinate system, O, is located at the center of the bottom node, and the X axis is pointed by the node where the origin O is located at the other node, the Z axis is straight up, and the Y axis is determined by the right hand rule.

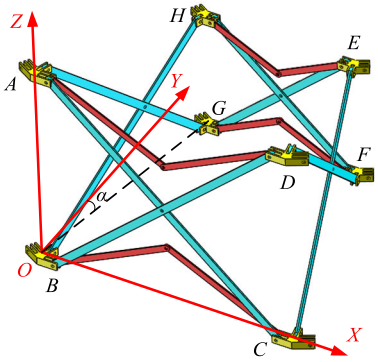

FIGURE 10. Closed loop deployable mechanism unit and coordinate system.

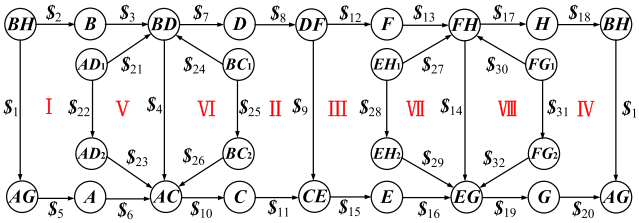

FIGURE 11. Screw constraint topological diagram of the closed loop deployable mechanism unit.

In the closed-loop deployable mechanism unit shown in Fig. 10, the number of rods is indicated by the number of the connected nodes. For example, the number of the scissors rods between nodes B and D is BD, and the two connected rods between nodes B and C are BC_1 and BC_2. Based on graph theory and screw theory, the components are represented by circles, the joints are represented by lines, and the motions at different joints are represented by the numerical unit twists. For instance, the motion of the joint between the scissors rods AC and BD is $\$_4$. The screw constraint topological diagram of the closed-loop deployable mechanism unit can then be obtained, as shown in Fig. 11.

The position coordinate of joint 4 connecting the scissors rod AC and BD can be obtained as follows:

$$r_4 = \begin{pmatrix} n + L\sin(\theta/2) & 0 & L\cos(\theta/2) \end{pmatrix} \tag{11}$$

The direction of the axis of joint 4 is:

$$S_4 = \begin{pmatrix} 0 & 1 & 0 \end{pmatrix} \tag{12}$$

According to screw theory, the unit twist of joint 4 is:

$$\$_4 = \begin{bmatrix} 0 & 1 & 0 & -L\cos(\theta/2) & 0 & n + L\sin(\theta/2) \end{bmatrix}^{\mathrm{T}} \tag{13}$$

Similarly, the expressions of the other unit twists shown in Fig. 10 can be obtained. We use ω to indicate the angular velocity value of the revolute joints in the double-hoop truss deployable mechanism. For the eight closed loops of I-VIII shown in Fig. 11, the corresponding screw constraint

equations can be established as follows:

$$\begin{cases} -\omega_1\$_1 + \omega_2\$_2 + \omega_3\$_3 + \omega_4\$_4 - \omega_5\$_5 - \omega_6\$_6 = \mathbf{0} \\ -\omega_4\$_4 + \omega_7\$_7 + \omega_8\$_8 + \omega_9\$_9 - \omega_{10}\$_{10} - \omega_{11}\$_{11} = \mathbf{0} \\ -\omega_9\$_9 + \omega_{12}\$_{12} + \omega_{13}\$_{13} \\ +\omega_{14}\$_{14} - \omega_{15}\$_{15} - \omega_{16}\$_{16} = \mathbf{0} \\ -\omega_{14}\$_{14} + \omega_{17}\$_{17} + \omega_{18}\$_{18} \\ +\omega_1\$_1 - \omega_{19}\$_{19} - \omega_{20}\$_{20} = \mathbf{0} \\ \omega_4\$_4 + \omega_{21}\$_{21} - \omega_{22}\$_{22} - \omega_{23}\$_{23} = \mathbf{0} \\ -\omega_4\$_4 - \omega_{24}\$_{24} + \omega_{25}\$_{25} + \omega_{26}\$_{26} = \mathbf{0} \\ \omega_{14}\$_{14} + \omega_{27}\$_{27} - \omega_{28}\$_{28} - \omega_{29}\$_{29} = \mathbf{0} \\ -\omega_{14}\$_{14} - \omega_{30}\$_{30} + \omega_{31}\$_{31} + \omega_{32}\$_{32} = \mathbf{0} \end{cases} \tag{14}$$

where ω_i represents the angular velocity of joint i, and $\mathbf{0}$ is a 6×1 null matrix.

Eq. (14) can be written in a matrix form as follows:

$$\boldsymbol{MN} = \mathbf{0} \tag{15}$$

where $\mathbf{0}$ is a 32×1 null matrix.

$$\boldsymbol{N} = \begin{bmatrix} \omega_1 & \omega_2 & \omega_3 & \dots & \dots & \omega_{30} & \omega_{31} & \omega_{32} \end{bmatrix}^T \tag{16}$$

$$\boldsymbol{M} = \begin{bmatrix} \boldsymbol{M}_2 & \boldsymbol{M}_1 & \boldsymbol{M}_1 & \boldsymbol{M}_1 \\ \boldsymbol{M}_3 & \boldsymbol{M}_4 & \boldsymbol{M}_1 & \boldsymbol{M}_1 \\ \boldsymbol{M}_1 & \boldsymbol{M}_5 & \boldsymbol{M}_1 & \boldsymbol{M}_1 \\ \boldsymbol{M}_6 & \boldsymbol{M}_7 & \boldsymbol{M}_8 & \boldsymbol{M}_1 \\ \boldsymbol{M}_9 & \boldsymbol{M}_1 & \boldsymbol{M}_{10} & \boldsymbol{M}_1 \\ -\boldsymbol{M}_9 & \boldsymbol{M}_1 & \boldsymbol{M}_{11} & \boldsymbol{M}_{12} \\ \boldsymbol{M}_1 & \boldsymbol{M}_{13} & \boldsymbol{M}_1 & \boldsymbol{M}_{14} \\ \boldsymbol{M}_1 & -\boldsymbol{M}_{13} & \boldsymbol{M}_1 & \boldsymbol{M}_{15} \end{bmatrix} \tag{17}$$

The expressions of all the symbols in Eq. (17) are as follows:

$$\begin{cases} \boldsymbol{M}_1 = \begin{pmatrix} \mathbf{0} & \mathbf{0} & \mathbf{0} & \mathbf{0} & \mathbf{0} & \mathbf{0} & \mathbf{0} & \mathbf{0} \end{pmatrix} \\ \boldsymbol{M}_2 = \begin{pmatrix} -\$_1 & \$_2 & \$_3 & \$_4 & -\$_5 & -\$_6 & \mathbf{0} & \mathbf{0} \end{pmatrix} \\ \boldsymbol{M}_3 = \begin{pmatrix} \mathbf{0} & \mathbf{0} & \mathbf{0} & -\$_4 & \mathbf{0} & \mathbf{0} & \$_7 & \$_8 \end{pmatrix} \\ \boldsymbol{M}_4 = \begin{pmatrix} \$_9 & -\$_{10} & -\$_{11} & \mathbf{0} & \mathbf{0} & \mathbf{0} & \mathbf{0} & \mathbf{0} \end{pmatrix} \\ \boldsymbol{M}_5 = \begin{pmatrix} -\$_9 & \mathbf{0} & \mathbf{0} & \$_{12} & \$_{13} & \$_{14} & -\$_{15} & -\$_{16} \end{pmatrix} \\ \boldsymbol{M}_6 = \begin{pmatrix} \$_1 & \mathbf{0} & \mathbf{0} & \mathbf{0} & \mathbf{0} & \mathbf{0} & \mathbf{0} & \mathbf{0} \end{pmatrix} \\ \boldsymbol{M}_7 = \begin{pmatrix} \mathbf{0} & \mathbf{0} & \mathbf{0} & \mathbf{0} & \mathbf{0} & -\$_{14} & \mathbf{0} & \mathbf{0} \end{pmatrix} \\ \boldsymbol{M}_8 = \begin{pmatrix} \$_{17} & \$_{18} & -\$_{19} & -\$_{20} & \mathbf{0} & \mathbf{0} & \mathbf{0} & \mathbf{0} \end{pmatrix} \\ \boldsymbol{M}_9 = \begin{pmatrix} \mathbf{0} & \mathbf{0} & \mathbf{0} & \$_4 & \mathbf{0} & \mathbf{0} & \mathbf{0} & \mathbf{0} \end{pmatrix} \\ \boldsymbol{M}_{10} = \begin{pmatrix} \mathbf{0} & \mathbf{0} & \mathbf{0} & \mathbf{0} & \$_{21} & -\$_{22} & -\$_{23} & \mathbf{0} \end{pmatrix} \\ \boldsymbol{M}_{11} = \begin{pmatrix} \mathbf{0} & \mathbf{0} & \mathbf{0} & \mathbf{0} & \mathbf{0} & \mathbf{0} & \mathbf{0} & -\$_{24} \end{pmatrix} \\ \boldsymbol{M}_{12} = \begin{pmatrix} \$_{25} & \$_{26} & \mathbf{0} & \mathbf{0} & \mathbf{0} & \mathbf{0} & \mathbf{0} & \mathbf{0} \end{pmatrix} \\ \boldsymbol{M}_{13} = \begin{pmatrix} \mathbf{0} & \mathbf{0} & \mathbf{0} & \mathbf{0} & \mathbf{0} & \$_{14} & \mathbf{0} & \mathbf{0} \end{pmatrix} \\ \boldsymbol{M}_{14} = \begin{pmatrix} \mathbf{0} & \mathbf{0} & \$_{27} & -\$_{28} & -\$_{29} & \mathbf{0} & \mathbf{0} & \mathbf{0} \end{pmatrix} \\ \boldsymbol{M}_{15} = \begin{pmatrix} \mathbf{0} & \mathbf{0} & \mathbf{0} & \mathbf{0} & \mathbf{0} & -\$_{30} & \$_{31} & \$_{32} \end{pmatrix} \end{cases} \tag{18}$$

where $\mathbf{0}$ is a 6×1 null matrix.

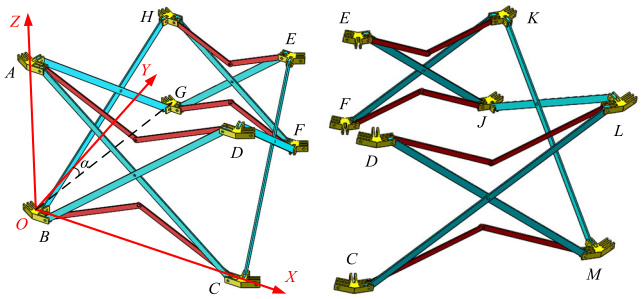

FIGURE 12. Combination mechanism and coordinate system.

The coefficient matrix $\boldsymbol{M}$ is a 48×32 dimensional matrix, the DOF of the closed loop deployable mechanism unit corresponds to the dimension of the null space of the coefficient matrix, and the rank of the coefficient matrix $\boldsymbol{M}$ can be calculated by the Matlab software:

$$rank\ (\boldsymbol{M}) = 31 \tag{19}$$

The number of columns in the matrix $\boldsymbol{M}$ is 32, so the number of the DOF of the closed-loop deployable mechanism unit is 1.

B. DOF ANALYSIS OF THE NON-CLOSED-LOOP DEPLOYABLE MECHANISM UNIT

There are N-2 identical non-closed-loop deployable mechanism units in the double-hoop truss deployable mechanism which contains N sides. To analyze the DOF of the non-closed-loop deployable mechanism unit, we combine this unit with a closed-loop deployable mechanism unit. The combination mechanism and the spatial coordinate system are shown in Fig. 12 which contains a closed-loop deployable mechanism unit and a non-closed-loop deployable mechanism unit.

Fig. 12 shows that the closed-loop deployable mechanism unit in the left is the same as the mechanism shown in Fig. 10. The nodes in the non-closed-loop deployable mechanism are also numbered by uppercase letters, and the numbering rules of the rods and revolute joints are the same as those for Fig. 10 and Fig. 11. Similarly, the screw constraint topological diagram of the non-closed loop deployable mechanism unit can be obtained, as shown in Fig. 13.

In Fig. 13, there are eight closed loops i-viii. The components and screws which are marked by the red dotted line in the closed loops i and iv belong to the closed loop deployable mechanism unit, so the two closed loops need to be removed when we establish the screw constraint equations, as shown in Eq. (20):

$$\begin{cases} -\omega_{34}\$_{34} + \omega_{36}\$_{36} + \omega_{37}\$_{37} \\ +\omega_{38}\$_{38} - \omega_{39}\$_{39} - \omega_{40}\$_{40} = \mathbf{0} \\ -\omega_{38}\$_{38} + \omega_{41}\$_{41} + \omega_{42}\$_{42} + \omega_{43}\$_{43} - \omega_{44}\$_{44} \\ -\omega_{45}\$_{45} = \mathbf{0} \\ \omega_{34}\$_{34} + \omega_{48}\$_{48} - \omega_{49}\$_{49} - \omega_{50}\$_{50} = \mathbf{0} \\ -\omega_{34}\$_{34} - \omega_{51}\$_{51} + \omega_{52}\$_{52} + \omega_{53}\$_{53} = \mathbf{0} \\ \omega_{43}\$_{43} + \omega_{54}\$_{54} - \omega_{55}\$_{55} - \omega_{56}\$_{56} = \mathbf{0} \\ -\omega_{43}\$_{43} - \omega_{57}\$_{57} + \omega_{58}\$_{58} + \omega_{59}\$_{59} = \mathbf{0} \end{cases} \tag{20}$$

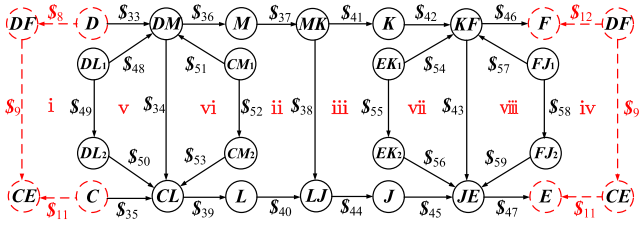

FIGURE 13. Screw constraint topological diagram of the non-closed loop deployable mechanism unit.

Eq. (20) can be written in a matrix form:

$$\boldsymbol{M'N'} = \mathbf{0} \tag{21}$$

Similarly to the above analysis, the coefficient matrix in Eq. (21) is a 36×27 dimensional matrix, and the rank of the coefficient matrix can also be calculated by the Matlab software:

$$rank\left(\boldsymbol{M'}\right) = 26 \tag{22}$$

It can be obtained that the number of the DOF of the non-closed loop deployable mechanism unit is also 1.

C. DOF ANALYSIS OF THE WHOLE DOUBLE-LOOP TRUSS DEPLOYABLE MECHANISM

The number of the DOF of both the closed-loop and non-closed-loop mechanism units is 1. In addition to these two mechanism units, there are also two overconstrained scissors deployable mechanism units in the double-hoop truss deployable mechanism. They are not independent, belonging to one mechanism unit. Similarly, the number of the DOF of the two overconstrained scissors deployable mechanism units obtained is also 1.

In the above analysis, the screw constraint equations correspond to the independent closed-loops in each mechanism unit. This is suitable for the single mechanism unit, but for the DOF analysis of the whole double-hoop truss deployable mechanism, it is necessary to establish the screw constraint equations for the shared closed loops between the mechanism units.

The screw constraint equations corresponding to the closed loops i and iv in Fig. 13 are:

$$\begin{cases} -\omega_8\$_8 - \omega_9\$_9 + \omega_{11}\$_{11} + \omega_{33}\$_{33} + \omega_{34}\$_{34} - \omega_{35}\$_{35} = \mathbf{0} \\ \omega_9\$_9 + \omega_{11}\$_{11} - \omega_{12}\$_{12} - \omega_{43}\$_{43} + \omega_{46}\$_{46} - \omega_{47}\$_{47} = \mathbf{0} \end{cases} \tag{23}$$

where $\mathbf{0}$ is a 6×1 null matrix.

Eq. (20) and Eq. (23) are combined and expressed the equations in a matrix form:

$$\boldsymbol{M''N''} = \mathbf{0} \tag{24}$$

where

$$\boldsymbol{N''} = \begin{bmatrix} \omega_8 & \omega_9 & \omega_{11} & \omega_{12} & \omega_{33} & \omega_{34} & \dots & \omega_{59} \end{bmatrix}^T \tag{25}$$

The coefficient matrix $\boldsymbol{M''}$ in Eq. (24) can be written in a partitioned matrix:

$$\boldsymbol{M''} = \begin{bmatrix} \boldsymbol{M''}_1 & \boldsymbol{M''}_2 \end{bmatrix} \tag{26}$$

where

$$\boldsymbol{M''}_1 = \begin{bmatrix} \mathbf{0} & \mathbf{0} & \mathbf{0} & \mathbf{0} & \mathbf{0} \\ \mathbf{0} & \mathbf{0} & \mathbf{0} & \mathbf{0} & \mathbf{0} \\ -\$_8 & -\$_9 & \mathbf{0} & \$_{11} & \mathbf{0} \\ \mathbf{0} & \$_9 & \mathbf{0} & \$_{11} & -\$_{12} \\ \mathbf{0} & \mathbf{0} & \mathbf{0} & \mathbf{0} & \mathbf{0} \\ \mathbf{0} & \mathbf{0} & \mathbf{0} & \mathbf{0} & \mathbf{0} \\ \mathbf{0} & \mathbf{0} & \mathbf{0} & \mathbf{0} & \mathbf{0} \\ \mathbf{0} & \mathbf{0} & \mathbf{0} & \mathbf{0} & \mathbf{0} \end{bmatrix} \tag{27}$$

$$\mathbf{M''}_2 = \begin{bmatrix} \boldsymbol{M''}_{22} & \boldsymbol{M''}_{21} & \boldsymbol{M''}_{21} \\ \boldsymbol{M''}_{23} & \boldsymbol{M''}_{24} & \boldsymbol{M''}_{21} \\ \boldsymbol{M''}_{25} & \boldsymbol{M''}_{21} & \boldsymbol{M''}_{21} \\ \boldsymbol{M''}_{21} & \boldsymbol{M''}_{26} & \boldsymbol{M''}_{21} \\ \boldsymbol{M''}_{27} & \boldsymbol{M''}_{28} & \boldsymbol{M''}_{21} \\ -\boldsymbol{M''}_{27} & \boldsymbol{M''}_{21} & \boldsymbol{M''}_{29} \\ \boldsymbol{M''}_{21} & \boldsymbol{M''}_{30} & \boldsymbol{M''}_{31} \\ \boldsymbol{M''}_{21} & -\mathbf{M''}_{30} & \boldsymbol{M''}_{32} \end{bmatrix} \tag{28}$$

In Eq. (28), the expressions for all the symbols are as follows:

$$\begin{cases} \boldsymbol{M''}_{21} = \begin{pmatrix} \mathbf{0} & \mathbf{0} & \mathbf{0} & \mathbf{0} & \mathbf{0} & \mathbf{0} & \mathbf{0} & \mathbf{0} & \mathbf{0} \end{pmatrix} \\ \boldsymbol{M''}_{22} = \begin{pmatrix} \mathbf{0} & -\$_{34} & \mathbf{0} & \$_{36} & \$_{37} & \$_{38} & -\$_{39} & -\$_{40} & \mathbf{0} \end{pmatrix} \\ \boldsymbol{M''}_{23} = \begin{pmatrix} \mathbf{0} & \mathbf{0} & \mathbf{0} & \mathbf{0} & \mathbf{0} & -\$_{38} & \mathbf{0} & \mathbf{0} & \$_{41} \end{pmatrix} \\ \boldsymbol{M''}_{24} = \begin{pmatrix} \$_{41} & \$_{42} & \$_{43} & -\$_{44} & -\$_{45} & \mathbf{0} & \mathbf{0} & \mathbf{0} & \mathbf{0} \end{pmatrix} \\ \boldsymbol{M''}_{25} = \begin{pmatrix} \$_{33} & \$_{34} & -\$_{35} & \mathbf{0} & \mathbf{0} & \mathbf{0} & \mathbf{0} & \mathbf{0} & \mathbf{0} \end{pmatrix} \\ \boldsymbol{M''}_{26} = \begin{pmatrix} \mathbf{0} & -\$_{43} & \mathbf{0} & \mathbf{0} & \$_{46} & -\$_{47} & \mathbf{0} & \mathbf{0} & \mathbf{0} \end{pmatrix} \\ \boldsymbol{M''}_{27} = \begin{pmatrix} \mathbf{0} & \$_{34} & \mathbf{0} & \mathbf{0} & \mathbf{0} & \mathbf{0} & \mathbf{0} & \mathbf{0} & \mathbf{0} \end{pmatrix} \\ \boldsymbol{M''}_{28} = \begin{pmatrix} \mathbf{0} & \mathbf{0} & \mathbf{0} & \mathbf{0} & \mathbf{0} & \mathbf{0} & \$_{48} & -\$_{49} & \$_{50} \end{pmatrix} \\ \boldsymbol{M''}_{29} = \begin{pmatrix} -\$_{51} & \$_{52} & \$_{53} & \mathbf{0} & \mathbf{0} & \mathbf{0} & \mathbf{0} & \mathbf{0} & \mathbf{0} \end{pmatrix} \\ \boldsymbol{M''}_{30} = \begin{pmatrix} \mathbf{0} & \$_{43} & \mathbf{0} & \mathbf{0} & \mathbf{0} & \mathbf{0} & \mathbf{0} & \mathbf{0} & \mathbf{0} \end{pmatrix} \\ \boldsymbol{M''}_{31} = \begin{pmatrix} \mathbf{0} & \mathbf{0} & \mathbf{0} & \$_{54} & -\$_{55} & -\$_{56} & \mathbf{0} & \mathbf{0} & \mathbf{0} \end{pmatrix} \\ \boldsymbol{M''}_{32} = \begin{pmatrix} \mathbf{0} & \mathbf{0} & \mathbf{0} & \mathbf{0} & \mathbf{0} & \mathbf{0} & -\$_{57} & \$_{58} & \$_{59} \end{pmatrix} \end{cases} \tag{29}$$

where $\mathbf{0}$ is a 6×1 null matrix.

Based on Fig. 11 and Fig. 13, the screw constraint topological diagram of the combination mechanism shown in Fig. 12 can be obtained. Combining Eq. (15) with Eq. (24), we can also obtain the screw constraint equations of the combination mechanism shown in Fig. 12:

$$\boldsymbol{PQ} = \mathbf{0} \tag{30}$$

where

$$\boldsymbol{Q} = \begin{bmatrix} \omega_1 & \omega_2 & \omega_3 & \dots & \dots & \omega_{57} & \omega_{58} & \omega_{59} \end{bmatrix}^T \tag{31}$$

The constraint matrix $\boldsymbol{P}$ can be easily obtained through Eq. (15) and Eq. (24). Based on Figs. 10-13, some joints and nodes are repeatedly calculated, so when the rank of the coefficient matrix is calculated, one of the constraint screws $\$_8$, $\$_9$, $\$_{11}$ and $\$_{12}$ should be removed. For convenience analysis without loss of generality, one of the doubling counting constraints, namely the matrix $\boldsymbol{M''}_1$, is removed from Eq. (26), and then the coefficient matrix can be rewritten as follows:

$$\boldsymbol{P'} = \begin{bmatrix} \boldsymbol{M} & \boldsymbol{0}_{48\times 27} \\ \boldsymbol{0}_{48\times 32} & \boldsymbol{M''}_2 \end{bmatrix} \tag{32}$$

It is well known that the rank of the diagonal matrix is equal to the sum of every matrix rank in matrix theory. Therefore, Eq. (32) is used to derive the following equation:

$$rank(\boldsymbol{P'}) = rank(\boldsymbol{M}) + rank(\boldsymbol{M''}_2) \tag{33}$$

Substituting the corresponding parameters, we obtain the following results:

$$\begin{cases} rank(\boldsymbol{M}) = 31 \\ rank(\boldsymbol{M''}_2) = 27 \end{cases} \tag{34}$$

The number of the DOF of the combination mechanism can be obtained as follows:

$$t = u - rank(\boldsymbol{P'}) = 59 - 58 = 1 \tag{35}$$

where t represents the number of the DOF, and u is the number of columns in the matrix.

The matrix $\boldsymbol{M''}_2$ is a full rank matrix, and Eq. (35) can also be written as follows:

$$\begin{aligned} t &= u_{\boldsymbol{M}} + u_{\boldsymbol{M''}_2} - rank(\boldsymbol{M}) - rank(\boldsymbol{M''}_2) \\ &= [u_{\boldsymbol{M}} - rank(\boldsymbol{M})] + \left[u_{\boldsymbol{M''}_2} - rank(\boldsymbol{M''}_2)\right] \\ &= u_{\boldsymbol{M}} - rank(\boldsymbol{M}) \end{aligned} \tag{36}$$

It can be seen from Eq. (36) that the DOF of the combination mechanism still depends on the matrix $\boldsymbol{M}$, the same as that of the closed-loop deployable mechanism unit.

To form the double-hoop truss deployable mechanism, we continue the addition of the rest of the N-2 non-closed loop deployable mechanism units and two overconstrained scissors mechanism units to the closed loop deployable mechanism, as shown in the above analysis. It can be concluded that the DOF still depends on the matrix $\boldsymbol{M}$, and that the DOF of the whole double-hoop truss deployable mechanism is 1, the same as that of the closed-loop deployable mechanism unit.

IV. VELOCITY ANALYSIS OF THE DOUBLE-HOOP TRUSS DEPLOYABLE MECHANISM

A. VELOCITY ANALYSIS OF THE CLOSED LOOP DEPLOYABLE MECHANISM UNIT

The DOF of the closed-loop deployable mechanism unit is 1, so when the input is given, the angular velocities in this unit can be solved through Eq. (14). Based on the scissors configuration geometry relationship and the screw constraint topological diagram in Fig. 11, the screw velocities of the components in the closed loop I can be expressed as follows:

$$\begin{cases} \boldsymbol{0} = \boldsymbol{V}_B \\ \omega_3\$_3 = \boldsymbol{V}_{BD} \\ -\omega_2\$_2 = \boldsymbol{V}_{BH} \\ \omega_1\$_1 - \omega_2\$_2 = \boldsymbol{V}_{AG} \\ \omega_3\$_3 + \omega_4\$_4 = \boldsymbol{V}_{AC} \\ \omega_1\$_1 - \omega_2\$_2 + \omega_5\$_5 = \boldsymbol{V}_A \end{cases} \tag{37}$$

where $\boldsymbol{0}$ is a 6×1 null matrix, and $\boldsymbol{V}_i$ represents the screw velocity of component i.

In the closed loop II shown in Fig. 11, the screw velocities of components BD and AC can be obtained through Eq. (37). Based on these two components, the screw velocities of the other components in the closed loop II can be obtained:

$$\begin{cases} \omega_3\$_3 = \boldsymbol{V}_{BD} \\ \omega_3\$_3 + \omega_4\$_4 = \boldsymbol{V}_{AC} \\ \boldsymbol{V}_{BD} + \omega_7\$_7 = \boldsymbol{V}_D \\ \boldsymbol{V}_{AC} + \omega_{10}\$_{10} = \boldsymbol{V}_C \\ \boldsymbol{V}_{BD} + \omega_7\$_7 + \omega_8\$_8 = \boldsymbol{V}_{DF} \\ \boldsymbol{V}_{AC} + \omega_{10}\$_{10} + \omega_{11}\$_{11} = \boldsymbol{V}_{CE} \end{cases} \tag{38}$$

Similarly, the screw velocities of the other components in the closed loops III-VIII shown in Fig. 11 can be obtained.

According to the physical meaning of the screw velocity, the angular velocity can be expressed as:

$$\boldsymbol{\omega}_i = \omega\left(\boldsymbol{V}_i\right) \tag{39}$$

where $\omega(\cdot)$ is a matrix representing the first three elements in the screw velocity.

The screw velocity contains two parts: the first three represent the angular velocity of the component, and the last three represent the linear velocity of the origin coincident point on the component. The linear velocity of the component can be expressed as:

$$\boldsymbol{v}_i = \nu\left(\boldsymbol{V}_i\right) + \omega\left(\boldsymbol{V}_i\right) \times \boldsymbol{r}_i \tag{40}$$

where $\nu(\cdot)$ is a matrix representing the last three elements in the screw velocity, and $\boldsymbol{r}_i$ is a vector from the origin of the coordinate to the centroid position of the component.

Through the above analysis and calculation, the angular velocity and linear velocity at the centroid of each component in the closed loop deployable mechanism unit can be obtained.

B. VELOCITY ANALYSIS OF THE OTHER MECHANISM UNITS

The double-hoop truss deployable mechanism is a completely symmetric mechanism, with each mechanism unit having the same structural dimensions and symmetric about the hoop center. If the coordinate systems at each of the mechanism units is established, the components located at the same position in their own coordinate systems of the mechanism units have the same velocity.

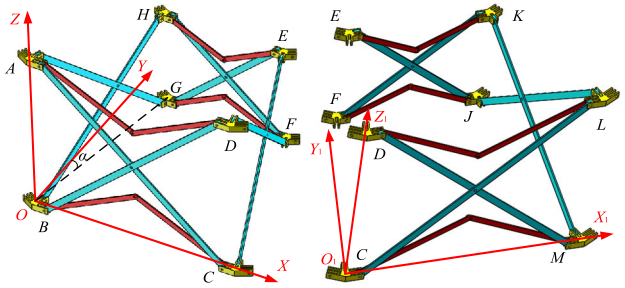

FIGURE 14. Combination mechanism and two coordinate systems.

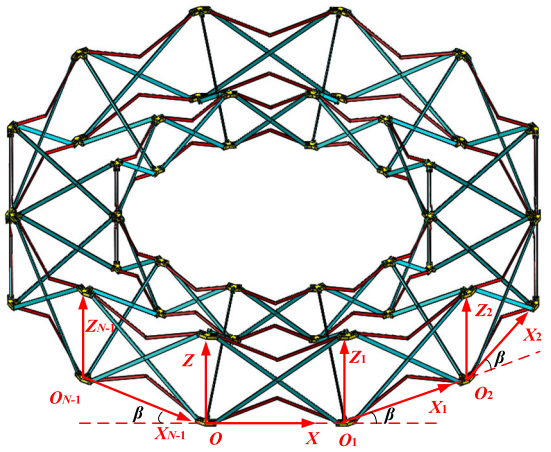

FIGURE 15. Double-hoop truss deployable mechanism and coordinate systems.

Similar to the system coordinate *O-XYZ* in the left mechanism unit in Fig. 14, the coordinate system O_1-$X_1Y_1Z_1$ is established at the same position in the right mechanism unit. The velocity of node C in the coordinate system *O-XYZ* is the same as that of node M in the coordinate system O_1-$X_1Y_1Z_1$:

$$\begin{cases} {}^{O}\boldsymbol{v}_C = {}^{O_1}\boldsymbol{v}_M \\ {}^{O}\boldsymbol{\omega}_C = {}^{O_1}\boldsymbol{\omega}_M \end{cases} \tag{41}$$

The equations in Eq. (41) can be extended to the whole double-hoop truss deployable mechanism. There are N mechanism units in total, on which the corresponding coordinate systems can be established, as shown in Fig. 15.

In Fig. 15, there total Ncoordinate systems in total numbered with *O-XYZ* to O_{N-1}-$X_{N-1}Y_{N-1}Z_{N-1}$. The coordinate system *O-XYZ* is selected to be the global coordinate system. The angle between the X axes of the adjacent coordinate systems is β, and the value of angle β can be calculated:

$$\beta = 360/N \tag{42}$$

The velocity of each component can be expressed in the global system:

$$\begin{cases} {}^{O}\boldsymbol{v}_i = {}^{O}_{O_j}\boldsymbol{R}\,{}^{O_j}\boldsymbol{v}_i + \sum_{k=1}^{j} {}^{O}_{O_{k-1}}\boldsymbol{R}\,{}^{O_{k-1}}\boldsymbol{v}_{O_k} \\ {}^{O}\boldsymbol{\omega}_i = {}^{O}_{O_j}\boldsymbol{R}\,{}^{O_j}\boldsymbol{\omega}_i + \sum_{k=1}^{j} {}^{O}_{O_{k-1}}\boldsymbol{R}\,{}^{O_{k-1}}\boldsymbol{\omega}_{O_k} \end{cases} \tag{43}$$

where i and j are the numbers of components and coordinate systems, respectively, and $\boldsymbol{R}$ is the rotational transform matrix.

The expression of matrix ${}^{O}_{O_j}\boldsymbol{R}$ is as follows:

$${}^{O}_{O_j}\boldsymbol{R} = \begin{bmatrix} \cos j\beta & -\sin j\beta & 0 \\ \sin j\beta & \cos j\beta & 0 \\ 0 & 0 & 1 \end{bmatrix} \tag{44}$$

where j is the number of the coordinate system.

The angular velocity and linear velocity of each component in the whole double-hoop truss deployable mechanism can then be solved and represented in the global coordinate system.

When the angular velocity and linear velocity of the components in the mechanism are obtained, the six-dimensional velocity vector of each component can be constructed through combining the angular velocity and linear velocity. The Jacobian matrix of each component can then be obtained through symbolic operation:

$$\boldsymbol{V'}_i = \begin{pmatrix} \boldsymbol{\omega}_i \\ \boldsymbol{v}_i \end{pmatrix} = \begin{pmatrix} \omega\left(\boldsymbol{V}_i\right) \\ v\left(\boldsymbol{V}_i\right) + \omega\left(\boldsymbol{V}_i\right) \times \boldsymbol{r}_i \end{pmatrix} = \boldsymbol{J}_i\left(\boldsymbol{\gamma}\right)\dot{\boldsymbol{\gamma}} \tag{45}$$

where $\boldsymbol{V'}_i$ represents the six-dimensional velocity of component i, γ is the input angle function and $\boldsymbol{J}_i\left(\boldsymbol{\gamma}\right)$ is the Jacobian matrix of component i.

V. ACCELERATION ANALYSIS OF THE DOUBLE-HOOP TRUSS DEPLOYABLE MECHANISM

The screw derivative is used to represent the acceleration of each component, indicating the acceleration of coincidence points of the reference coordinate system on the component [44]. The formula of the screw acceleration is:

$$\boldsymbol{A}_i = \begin{pmatrix} \boldsymbol{\varepsilon}_i \\ \boldsymbol{a} - \boldsymbol{\omega} \times \boldsymbol{v} \end{pmatrix} \tag{46}$$

where $\boldsymbol{A}_i$ is the screw acceleration of component i, $\boldsymbol{\varepsilon}_i$ is the angular acceleration, and $\boldsymbol{a}$ is the linear acceleration of the centroid point of component i.

The screw acceleration synthesis rule for a multibody system is:

$${}^{0}\boldsymbol{A}_{0n} = \sum_{i=0}^{n-1} {}^{0}\boldsymbol{A}_{i(i+1)} + \sum_{i=0}^{n-2}\sum_{j=i+1}^{n-1} Lie\left[{}^{0}\boldsymbol{V}_{i(i+1)}, {}^{0}\boldsymbol{V}_{j(j+1)}\right] \tag{47}$$

where the "*Lie*[]" represents the Lie bracket operation.

If there are two screws:

$$\begin{cases} \$_1 = (\boldsymbol{s}_1; \boldsymbol{s}_{01}) \\ \$_2 = (\boldsymbol{s}_2; \boldsymbol{s}_{02}) \end{cases} \tag{48}$$

The rule of the Lie bracket operation is:

$$Lie\left[\$_1, \$_2\right] = \begin{pmatrix} \boldsymbol{s}_1 \times \boldsymbol{s}_2 \\ \boldsymbol{s}_1 \times \boldsymbol{s}_{02} - \boldsymbol{s}_2 \times \boldsymbol{s}_{01} \end{pmatrix} \tag{49}$$

For the closed loop I in Fig. 11, there are the following equations:

$$\begin{cases} \varepsilon_3\$_3 + \varepsilon_4\$_4 + \$^1_{Lie} = {}_B\boldsymbol{\varepsilon}_{AC} \\ -\varepsilon_2\$_2 + \varepsilon_1\$_1 + \varepsilon_5\$_5 + \varepsilon_6\$_6 + \$^2_{Lie} = {}_B\boldsymbol{\varepsilon}_{AC} \end{cases} \tag{50}$$

where

$$\begin{cases} \$^1_{Lie} = Lie\left[\omega_3\$_3, \omega_4\$_4\right] \\ \$^2_{Lie} = Lie\left[-\omega_2\$_2, \omega_1\$_1\right] + Lie\left[-\omega_2\$_2, \omega_5\$_5\right] \\ \quad + Lie\left[-\omega_2\$_2, \omega_6\$_6\right] \\ \quad + Lie\left[\omega_1\$_1, \omega_5\$_5\right] + Lie\left[\omega_1\$_1, \omega_6\$_6\right] + Lie\left[\omega_5\$_5, \omega_6\$_6\right] \end{cases} \tag{51}$$

The following equation can then be obtained:

$$\varepsilon_3\$_3 + \varepsilon_4\$_4 + \$^1_{Lie} + \varepsilon_2\$_2 - \varepsilon_1\$_1 - \varepsilon_5\$_5 - \varepsilon_6\$_6 - \$^2_{Lie} = \mathbf{0} \tag{52}$$

Similarly, the screw equations of the closed loop II-VIII in Fig. 11 can also obtained. When the input angular acceleration is given, such as $\boldsymbol{\varepsilon}_1$, the remaining angular accelerations can be solved.

According to the physical meaning of the screw acceleration, the angular acceleration and linear acceleration of each component can be expressed as:

$$\begin{cases} \boldsymbol{\varepsilon}_i = \varepsilon\left(\varepsilon_i\$_i\right) \\ \boldsymbol{a}_i = \left[a\left(\varepsilon_i\$_i\right) + \boldsymbol{\omega}_i \times \boldsymbol{v}_i\right] + \left[\varepsilon\left(\varepsilon_i\$_i\right) \times \boldsymbol{r}_i\right] + \left[\boldsymbol{\omega}_i \times \left(\boldsymbol{\omega}_i \times \boldsymbol{r}_i\right)\right] \end{cases} \tag{53}$$

where $\varepsilon(\cdot)$ is a matrix representing the first three elements in the screw acceleration, and $a(\cdot)$ is a matrix representing the last three elements in the screw acceleration.

The analysis in Section IV shows that the components at the same position in each mechanism unit have the same acceleration in their own coordinate systems. The acceleration of each component can then be expressed in the global coordinate system:

$$\begin{cases} {}^O\boldsymbol{\varepsilon}_i = {}^O_{O_j}\boldsymbol{R}^{O_j}\boldsymbol{\varepsilon}_i + \sum_{k=1}^{j} {}^O_{O_{k-1}}\boldsymbol{R}^{O_{k-1}}\boldsymbol{\varepsilon}_{O_k} \\ {}^O\boldsymbol{a}_i = {}^O_{O_j}\boldsymbol{R}^{O_j}\boldsymbol{a}_i + \sum_{k=1}^{j} {}^O_{O_{k-1}}\boldsymbol{R}^{O_{k-1}}\boldsymbol{a}_{O_k} \end{cases} \tag{54}$$

The above analysis and calculation show that the angular acceleration and linear acceleration of each component in the whole double-hoop truss deployable mechanism can be solved and represented in the global coordinate system.

VI. DYNAMIC MODELING AND NUMERICAL SIMULATION OF THE DOUBLE-HOOP TRUSS DEPLOYABLE MECHANISM

A. DYNAMIC MODELING

According to Newton-Euler equation, the relationship between the external force and torque of the component and its linear acceleration and angular acceleration is:

$$\begin{cases} \boldsymbol{f} = \boldsymbol{ma} \\ \boldsymbol{\tau} = \boldsymbol{I\varepsilon} + \boldsymbol{\omega} \times \boldsymbol{I\omega} \end{cases} \tag{55}$$

where $\boldsymbol{f}$ and τ are the external force and torque, respectively, and $\boldsymbol{I}$ is the inertia tensor matrix of the component.

The inertial force of each component can be expressed as:

$$\boldsymbol{f}_i = -\boldsymbol{m}_i\boldsymbol{a}_i \tag{56}$$

where $\boldsymbol{m}_i$ and $\boldsymbol{a}_i$ represent the mass and the centroid linear acceleration of component i, respectively.

The inertial torque of each component can be expressed as:

$$\boldsymbol{\tau}_i = -\left(\boldsymbol{R}_i\boldsymbol{I}_i\boldsymbol{R}_i^T\boldsymbol{\varepsilon}_i + \boldsymbol{\omega}_i \times \left(\boldsymbol{R}_i\boldsymbol{I}_i\boldsymbol{R}_i^T\boldsymbol{\omega}_i\right)\right) \tag{57}$$

where $\boldsymbol{R}_i$ is the rotational transform matrix of component i, which can transform the inertia tensor matrix of the component into the global coordinate system.

For the components in the closed-loop deployable mechanism unit, their inertial force and inertial torque can be calculated by Eq. (56) and Eq. (57), respectively. For the components in the other mechanism units, their inertial force can also be calculated by Eq. (56); however, but when their inertial torque is calculated, it is necessary to add a rotational transform matrix, as shown in the following equation:

$$\boldsymbol{\tau}_i = -\left(\boldsymbol{R}_i{}^O_{O_j}\boldsymbol{R}\boldsymbol{I}_i\boldsymbol{R}_i^T\boldsymbol{\varepsilon}_i + \boldsymbol{\omega}_i \times \left(\boldsymbol{R}_i{}^O_{O_j}\boldsymbol{R}\boldsymbol{I}_i\boldsymbol{R}_i^T\boldsymbol{\omega}_i\right)\right) \tag{58}$$

Since the working environment of deployable antenna is in-orbit space, the influence of gravity can be ignored. The inertial force and torque of each component can be combined into a six-dimensional force vector:

$$\boldsymbol{F}_i = \begin{bmatrix} \boldsymbol{\tau}_i \\ \boldsymbol{f}_i \end{bmatrix} \tag{59}$$

Based on the virtual work principle and Eq. (45), the inverse dynamics equation of the double-hoop truss deployable mechanism can be obtained:

$$\boldsymbol{T} + \sum \boldsymbol{J}_i^T\boldsymbol{F}_i = \mathbf{0} \tag{60}$$

where $\boldsymbol{T}$ is the input driving torque.

Through Eq. (60), we can obtain the relationship between the input driving torque and the kinematic characteristics of the double-hoop truss deployable mechanism.

B. NUMERICAL SIMULATION

In order to verify the correctness of the above theoretical analysis, the simulation software Adams and the numerical calculation software Matlab are used to simulate and analyze the double-hoop truss deployable mechanism. Since the whole mechanism has a single DOF, just one driving input is needed. The simulation model is shown in Fig.16.

Fig. 16 shows the fully folded state of the double-hoop truss deployable mechanism. The theoretical analysis can be verified by the deploying process. There are seven types of components in the whole deployable mechanism, including three types of scissors rods, two types of connected rods and two types of nodes, as shown in Fig. 17.

Set the sides of the double-hoop truss deployable mechanism as 12, and the structural and physical parameters of this mechanism are shown in Table 1.

The theoretical model derived from the above analysis and the parameters shown in the Table 1 are used to obtain the

TABLE 1. Structural and physical parameters.

Parameter	Value
Length of the inner scissors rod (mm)	353.27
Length of the outer scissors rod (mm)	600
Length of the connected scissors rod (mm)	476.64
Length of the inner connected rod (mm)	147.20
Length of the outer connected rod (mm)	250
Distance between R joint and center in inner node (mm)	16.16
Distance between R joint and center in outer node (mm)	30.50
Mass of the inner scissors rod (kg)	0.13
Mass of the outer scissors rod (kg)	0.22
Mass of the connected scissors rod (kg)	0.18
Mass of the inner connected rod (kg)	0.04
Mass of the outer connected rod (kg)	0.06
Mass of the inner node (kg)	0.08
Mass of the outer node (kg)	0.11
Inertia tensor matrix of the inner scissors rod (kg/mm^2)	diag (1601.62 1599.29 2.65)
Inertia tensor matrix of the outer scissors rod (kg/mm^2)	diag (7209.40 7205.51 4.34)
Inertia tensor matrix of the connected scissors rod (kg/mm^2)	diag (3729.26 3726.15 3.50)
Inertia tensor matrix of the inner connected rod (kg/mm^2)	diag (78.05 77.63 0.48)
Inertia tensor matrix of the outer connected rod (kg/mm^2)	diag (349.29 348.59 0.78)
Inertia tensor matrix of the inner node (kg/mm^2)	diag (18.14 14.27 7.03)
Inertia tensor matrix of the outer node (kg/mm^2)	diag (40.94 33.02 12.13)
Initial folding angle of the scissors rods (°)	5.17
Input angle function	0.25t^2
Simulation time (s)	14.6

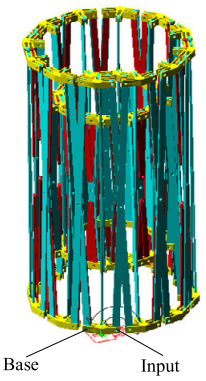

FIGURE 16. Simulation model of the double-hoop truss deployable antenna mechanism.

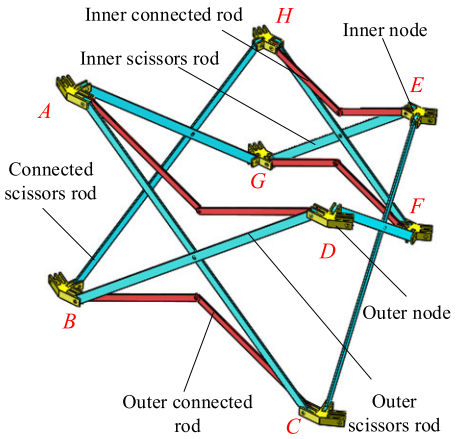

FIGURE 17. Seven types of components in the double-hoop truss deployable mechanism.

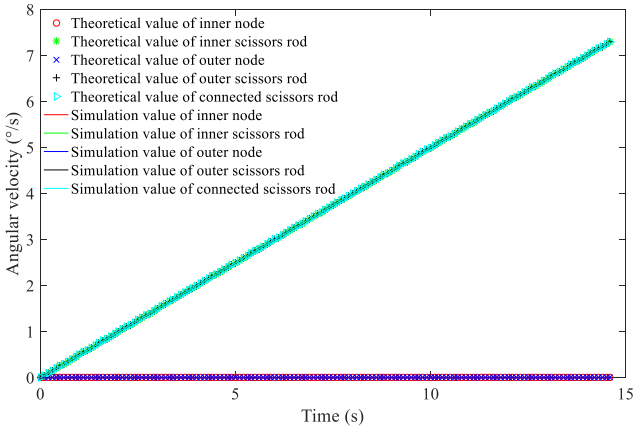

FIGURE 18. Angular velocities of the components.

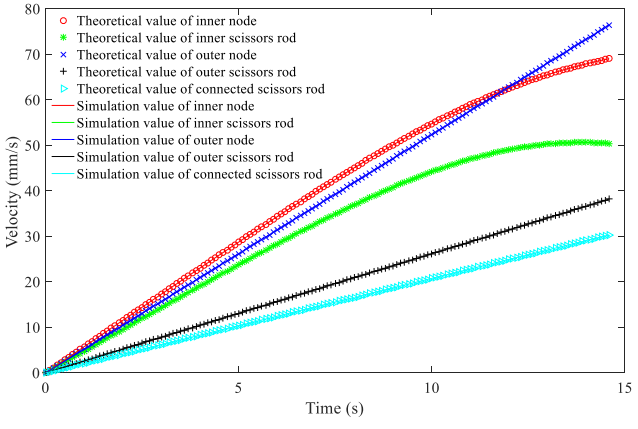

FIGURE 19. Linear velocities of the components.

theoretical calculation and simulation results. Because of too many components in the whole double-hoop truss deployable mechanism, we choose several typical components to perform the verification. As shown in Fig.15 and Fig. 17, we select the closed loop deployable mechanism unit whose coordinate system coincides with that of the global coordinate mechanism to be analyzed and calculated. Assume that the mechanism unit shown in Fig. 17 is the selected mechanism, and that the coordinate system is located at node *B*. Then we choose node *E*, the inner scissors rod *EG*, the connected scissors rod *BH*, the outer scissors rod *BD* and the outer node *D* for analysis and simulation. The angular velocity, linear velocity, angular acceleration, linear acceleration of the selected components, and the input driving torque of the whole mechanism are shown in Figs. 18-22.

Figs. 18-22, show that the curves of theoretical values of the components are exactly same as the curves of

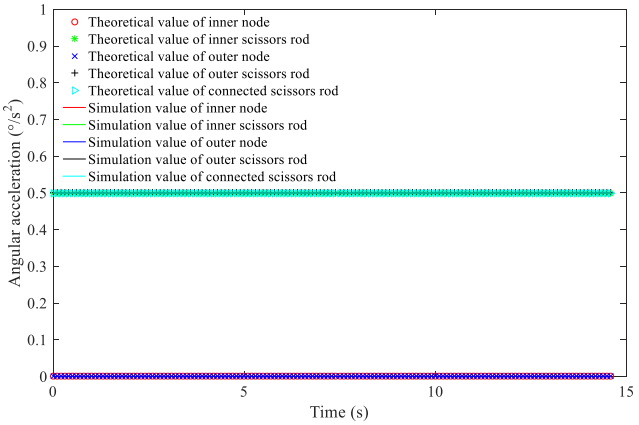

FIGURE 20. Angular accelerations of the components.

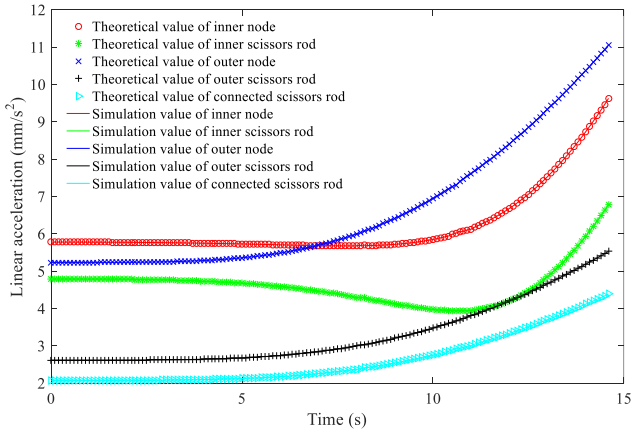

FIGURE 21. Linear accelerations of the components.

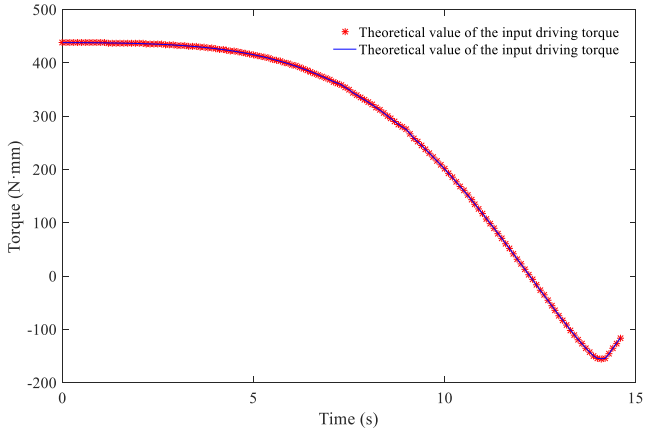

FIGURE 22. Input driving torque.

simulation values. Therefore, the correctness of the theoretical analysis can be verified.

It can be seen from Fig.18 and Fig.20 that during the deploying movement of the double-hoop truss deployable mechanism, the angular velocity and angular acceleration of the nodes are zero. That is, each node moves but has no rotation, which is consistent with the one DOF of the whole double-hoop truss deployable mechanism obtained in this study.

VII. CONCLUSION

Hoop truss deployable antenna is an important type in large-scale space antennas. In this paper, a double-hoop truss deployable antenna mechanism is proposed based on the overconstrained scissors mechanism. The configuration features and geometric conditions of this mechanism are analyzed with screw theory. The DOFs of the mechanism units and of the whole double-hoop truss deployable mechanism are investigated, showing that the whole mechanism has only one DOF. The kinematics of the double-hoop truss deployable mechanism are then analyzed, and the angular and linear velocities and accelerations of the components and the Jacobian matrixes are obtained. Finally, a dynamic model of the double-hoop truss deployable mechanism is established based on Newton-Euler equation and the principle of virtual work. The numerical simulation verifies the theoretical analysis.

The overconstrained scissors double-hoop truss deployable antenna mechanism proposed in this paper has the characteristics of single DOF, high structural stiffness and large load capacity; therefore, it has a good application prospect in the field of aerospace. The theoretical analysis method based on screw theory in this paper has clear physical meaning, which can be easily used to program calculation, and it can be well applied to other complex spatial deployable mechanisms.

REFERENCES

[1] G. Li, H. Huang, H. Guo, and B. Li, "Dynamic modeling and control for a deployable grasping manipulator," *IEEE Access*, vol. 7, pp. 23000–23011, 2019.
[2] F. Hu, Y. Song, Z. Huang, W. Liu, and W. Li, "Malleability and optimization of tetrahedral metamorphic element for deployable truss antenna reflector," *AIP Adv.*, vol. 8, no. 5, May 2013, Art. no. 055217.
[3] Y. Chen, J. Feng, and Q. Sun, "Lower-order symmetric mechanism modes and bifurcation behavior of deployable bar structures with cyclic symmetry," *Int. J. Solids Struct.*, vols. 139–140, pp. 1–14, May 2018.
[4] T. Li, J. Jiang, T. Shen, and Z. Wang, "Analysis of mechanical properties of wire mesh for mesh reflectors by fractal mechanics," *Int. J. Mech. Sci.*, vol. 92, pp. 90–97, Mar. 2015.
[5] K. Roovers and N. De Temmerman, "Deployable scissor grids consisting of translational units," *Int. J. Solids Struct.*, vol. 121, pp. 45–61, Aug. 2017.
[6] S. Pellegrino, "Deployable structures in engineering," in *Deployable Structures*. Berlin, Germany: Springer, 2001, pp. 1–35.
[7] B. Han, Y. Xu, J. Yao, W. Liu, X. Li, and Y. Zhao, "Design and analysis of the scissors double-ring truss deployable antenna mechanism," in *Proc. Asian Conf. Mech. Mach. Sci.*, Guangzhou, China, 2017, pp. 787–799.
[8] J. Santiago-Prowald and H. Baier, "Advances in deployable structures and surfaces for large apertures in space," *CEAS Space J.*, vol. 5, nos. 3–4, pp. 89–115, 2013.
[9] H. Guo, C. Shi, M. Li, Z. Deng, and R. Liu, "Design and dynamic equivalent modeling of double-layer hoop deployable antenna," *Int. J. Aerosp. Eng.*, vol. 2018, Jan. 2018, Art. no. 2941981.
[10] A. Meguro, A. Tsujihata, N. Hamamoto, and M. Homma, "Technology status of the 13 m aperture deployment antenna reflectors for engineering test satellite VIII," *Acta Astron.*, vol. 47, nos. 2–9, pp. 147–152, Jul./Nov. 2000.
[11] F. Hu, Y.-P. Song, S.-K. Zheng, Z.-R. Huang, and J. Zhu, "Advances and trends in space truss deployable antenna," *Yuhang Xuebao*, vol. 39, no. 2, pp. 111–120, Feb. 2018.
[12] S. Lu, D. Zlatanov, X. Ding, and R. Molfino, "A new family of deployable mechanisms based on the Hoekens linkage," *Mech. Mach. Theory*, vol. 73, pp. 130–153, Mar. 2014.

[13] K. K. Vu, J. R. Liew, and K. Anandasivam, "Deployable tension-strut structures: From concept to implementation," *J. Construct. Steel Res.*, vol. 62, no. 3, pp. 195–209, Mar. 2006.
[14] Y. Chen and Z. You, "On mobile assemblies of Bennett linkages," *Proc. Roy. Soc. A, Math. Phys. Eng. Sci.*, vol. 464, no. 2093, pp. 1275–1293, May 2008.
[15] Y. Chen, Z. You, and T. Tarnai, "Threefold-symmetric Bricard linkages for deployable structures," *Int. J. Solids Struct.*, vol. 42, no. 8, pp. 2287–2301, Apr. 2005.
[16] S. Hao, W. Dawei, K. Rongjie, and C. Yan, "Gait analysis and control of a deployable robot," *Mech. Mach. Theory*, vol. 120, pp. 107–119, Feb. 2018.
[17] X. Qi, Z. Deng, B. Li, R. Liu, and H. Guo, "Design and optimization of large deployable mechanism constructed by Myard linkages," *CEAS Space J.*, vol. 5, nos. 3–4, pp. 147–155, 2013.
[18] B. Han, Y. Xu, J. Yao, D. Zheng, S. Zhang, and Y. Zhao, "Kinematic characteristics analysis and assembly application of a spatial asymmetric 7R mechanism," *Hangkong Xuebao*, vol. 40, no. 4, Apr. 2019, Art. no. 422536.
[19] G. E. B. Tan and S. Pellegrino, "Nonlinear vibration of cable-stiffened pantographic deployable structures," *J. Sound Vib.*, vol. 314, nos. 3–5, pp. 783–802, Jul. 2008.
[20] Z. You and S. Pellegrino, "Cable-stiffened pantographic deployable structures part 2: Mesh reflector," *AIAA J.*, vol. 35, no. 8, pp. 1348–1355, Aug. 1997.
[21] Z. You, "Deployable structure of curved profile for space antennas," *J. Aerosp. Eng.*, vol. 13, no. 4, pp. 139–143, Oct. 2000.
[22] G. Liu, W. Chen, W. Wang, and Y. Chen, "Design and analysis of a novel space deployable mechanism of ring and frustum type," *Int. J. Adv. Manuf. Technol.*, vol. 94, nos. 9–12, pp. 3251–3264, Feb. 2018.
[23] M. Salar, M. R. Ghasemi, and B. Dizangian, "Practical optimization of deployable and scissor-like structures using a fast GA method," *Frontiers Struct. Civil Eng.*, vol. 13, no. 3, pp. 557–568, 2019. doi: 10.1007/s11709-018-0497-z.
[24] G. Fu-Ling, S. Jian-Jun, H. Guo-Yong, and Z. Jing-Jie, "Static analysis of synchronism deployable antenna," *J. Zhejiang Univ.-Sci. A*, vol. 7, no. 8, pp. 1365–1371, Aug. 2006.
[25] Y. Xu and F.-L. Guan, "Structure-electronic synthesis design of deployable truss antenna," *Aerosp. Sci. Technol.*, vol. 26, no. 1, pp. 259–267, Apr./May 2013.
[26] Y. Xu, F. Guan, X. Xu, H. Wang, and Y. Zheng, "Development of a novel double-ring deployable mesh antenna," *Int. J. Antennas Propag.*, vol. 2012, Oct. 2012, Art. no. 375463.
[27] L. Dai, F. Guan, and J. K. Guest, "Structural optimization and model fabrication of a double-ring deployable antenna truss," *Acta Astron.*, vol. 94, no. 2, pp. 843–851, 2014.
[28] Y. Xu, F.-L. Guan, Y. Zheng, and M. Zhao, "Kinematic analysis of the deployable truss structures for space applications," *J. Aerosp. Technol. Manage.*, vol. 4, no. 4, pp. 453–462, Oct. 2012.
[29] Z. Deng, H. Huang, B. Li, and R. Liu, "Synthesis of deployable/foldable single loop mechanisms with revolute joints," *J. Mech. Robot.*, vol. 3, no. 3, 2011, Art. no. 031006.
[30] Y. Wang, Z. Deng, R. Liu, H. Yang, and H. Guo, "Topology structure synthesis and analysis of spatial pyramid deployable truss structures for satellite SAR antenna," *Chin. J. Mech. Eng.*, vol. 27, no. 4, pp. 683–692, Jul. 2014.
[31] Z. Chu, Z. Deng, X. Qi, and B. Li, "Modeling and analysis of a large deployable antenna structure," *Acta Astron.*, vol. 95, pp. 51–60, Feb./Mar. 2014.
[32] D.-J. Zhao, J.-S. Zhao, and Z.-F. Yan, "Planar deployable linkage and its application in overconstrained lift mechanism," *J. Mech. Robot.*, vol. 8, no. 2, 2016, Art. no. 021022.
[33] Z. Huang, Q. Li, and H. Ding, "Mobility analysis part-1," in *Theory of Parallel Mechanisms*. Berlin, Germany: Springer, 2013, pp. 47–69.
[34] T. Li, H. Deng, and L. Zhang, "Mobility analysis of generalized mechanisms via screw algebra," in *Proc. Asian Conf. Mech. Mach. Sci.*, Guangzhou, China, 2017, pp. 581–596.
[35] Z. Huang, Q. Li, and H. Ding, "Mobility analysis part-2," in *Theory of Parallel Mechanisms*, Berlin, Germany: Springer, 2013, pp. 71–133.
[36] G. Gogu, "Mobility of mechanisms: A critical review," *Mech. Mach. Theory*, vol. 40, no. 9, pp. 1068–1097, Sep. 2005.
[37] J. S. Dai, Z. Huang, and H. Lipkin, "Mobility of overconstrained parallel mechanisms," *J. Mech. Des.*, vol. 128, no. 1, pp. 220–229, Jan. 2006.
[38] Z. Huang, J. Liu, and D. Zeng, "A general methodology for mobility analysis of mechanisms based on constraint screw theory," *Sci. China E, Technol. Sci.*, vol. 52, no. 5, pp. 1337–1347, May 2009.
[39] J.-S. Zhao, F. Chu, and Z.-J. Feng, "The mechanism theory and application of deployable structures based on SLE," *Mech. Mach. Theory*, vol. 44, no. 2, pp. 324–335, Feb. 2009.
[40] Y. Xu, W. Liu, L. Chen, J. Yao, Y. Zhao, and J. Zhu, "Mobility analysis of a deployable truss-antenna mechanism-method based on link-demolishing and equivalent idea," *Hongkong Xuebao*, vol. 38, no. 9, Sep. 2009, Art. no. 421188.
[41] G. Wei, X. Ding, and J. S. Dai, "Mobility and geometric analysis of the Hoberman switch-pitch ball and its variant," *J. Mech. Robot.*, vol. 2, no. 3, Aug. 2010, Art. no. 031010.
[42] Y. Sun, S. Wang, J. Li, and C. Zhi, "Mobility analysis of the deployable structure of SLE based on screw theory," *Chin. J. Mech. Eng.*, vol. 26, no. 4, pp. 793–800, Jul. 2013.
[43] J. Gallardo, J. M. Rico, A. Frisoli, D. Checcacci, and M. Bergamasco, "Dynamics of parallel manipulators by means of screw theory," *Mech. Mach. Theory*, vol. 38, no. 11, pp. 1113–1131, Nov. 2003.
[44] J. Gallardo-Alvarado, "Kinematics of a hybrid manipulator by means of screw theory," *Multibody Syst. Dyn.*, vol. 14, nos. 3–4, pp. 345–366, Nov. 2005.
[45] J. Gallardo-Alvarado, H. Orozco-Mendoza, R. Rodríguez-Castro, and J. M. Rico-Martínez, "Kinematics of a class of parallel manipulators which generates structures with three limbs," *Multibody Syst. Dyn.*, vol. 17, no. 1, pp. 27–46, Feb. 2007.
[46] J. Gallardo-Alvarado, *Kinematic Analysis of Parallel Manipulators by Algebraic Screw Theory*. Berlin, Germany: Springer, 2016, pp. 1–377.
[47] J. Gallardo-Alvarado, R. Rodríguez-Castro, and P. J. Delossantos-Lara, "Kinematics and dynamics of a 4-PRUR Schönflies parallel manipulator by means of screw theory and the principle of virtual work," *Mech. Mach. Theory*, vol. 122, pp. 347–360, Apr. 2018.
[48] J. Gallardo-Alvarado, C. R. Aguilar-Nájera, L. Casique-Rosas, J. M. Rico-Martínez, and M. NazrulIslam, "Kinematics and dynamics of 2(3-RPS) manipulators by means of screw theory and the principle of virtual work," *Mech. Mach. Theory*, vol. 43, no. 10, pp. 1281–1294, 2008.
[49] J. Gallardo-Alvarado and J. Rico-Martínez, "Kinematics of a hyper-redundant manipulator by means of screw theory," *Proc. Inst. Mech. Eng. K, J. Multi-Body Dyn.*, vol. 223, no. 4, pp. 325–334, Dec. 2010.
[50] S. J. Zhu, Z. Huang, and H. F. Ding, "Forward/reverse velocity and acceleration analysis for a class of lower-mobility parallel mechanisms," *J. Mech. Des.*, vol. 129, no. 4, pp. 390–396, Apr. 2007.
[51] H. Liu, T. Huang, and D. G. Chetwynd, "An approach for acceleration analysis of lower mobility parallel manipulators," *J. Mech. Robot.*, vol. 3, no. 1, Feb. 2011, Art. no. 011013.
[52] T. Zhao, M. Geng, Y. Chen, E. Li, and J. Yang, "Kinematics and dynamics Hessian matrices of manipulators based on screw theory," *Chin. J. Mech. Eng.*, vol. 28, no. 2, pp. 226–235, Mar. 2015.
[53] Y. Sun, S. Wang, J. K. Mills, and C. Zhi, "Kinematics and dynamics of deployable structures with scissor-like-elements based on screw theory," *Chin. J. Mech. Eng.*, vol. 27, no. 4, pp. 655–662, Jul. 2014.

BO HAN received the B.S. degree in mechanical engineering from the School of Mechanical Engineering, Yanshan University, Qinhuangdao, China, in 2014, where he is currently pursuing the Ph.D. degree in mechatronics engineering. His research interests include spatial deployable mechanism design and application, parallel mechanism theory and application, and multibody system dynamics.

DONG ZHENG received the B.S. degree in vehicle engineering from the School of Vehicles and Energy, Yanshan University, Qinhuangdao, China, in 2017, where he is currently pursuing the M.S. degree in mechatronics engineering. His research interests include spatial deployable antenna mechanism design and flexible multibody system dynamics.

YUNDOU XU received the Ph.D. degree in mechatronics engineering from the School of Mechanical Engineering, Yanshan University, Qinhuangdao, China, in 2012, where he is currently an Associate Professor with the Department of Mechatronics Engineering. He is also with the Parallel Robot and Mechatronic System Laboratory of Hebei Province, Yanshan University, and with the Key Laboratory of Advanced Forging and Stamping Technology and Science of Ministry of National Education, Yanshan University. His research interests include parallel mechanism theory and application, forging manipulators, and deployable antenna mechanism theory and application.

JIANTAO YAO received the Ph.D. degree in mechatronics engineering from the School of Mechanical Engineering, Yanshan University, Qinhuangdao, China, in 2009, where he is currently a Professor with the Department of Mechatronics Engineering. He is also with the Parallel Robot and Mechatronic System Laboratory of Hebei Province, Yanshan University, and with the Key Laboratory of Advanced Forging and Stamping Technology and Science of Ministry of National Education, Yanshan University. His research interests include soft robots, parallel six-axis force sensors, and parallel manipulators.

YONGSHENG ZHAO was born in Longjing, Jilin, China, in 1962. He received the B.S. degree in mechanical manufacturing process and equipment and the M.S. and Ph.D. degrees in mechanical design from the School of Mechanical Engineering, Yanshan University, Qinhuangdao, China, in 1983, 1987, and 1999, respectively, where he is currently a Professor with the Department of Mechatronics Engineering. He is also with the Parallel Robot and Mechatronic System Laboratory of Hebei Province, Yanshan University, and with the Key Laboratory of Advanced Forging and Stamping Technology and Science of Ministry of National Education, Yanshan University. His research interests include parallel mechanism theory and application, spatial deployable mechanism design and application, aerospace equipment and mechatronics systems, and advanced manufacturing technology.